Analytica Chimica Acta: X 2 (2019) 100017

Contents lists available at ScienceDirect

Analytica Chimica Acta: X

journal homepage: www.journals.elsevier.com/analytica-chimica-acta-x

Evaluation of the selectivity of G-quadruplex ligands in living cells with a small molecule fluorescent probe

Suge Zhang [a, b], Hongxia Sun [a, *], Dawei Yang [c], Yan Liu [a], Xiufeng Zhang [c], Hongbo Chen [a, b], Qian Li [a], Aijiao Guan [a], Yalin Tang [a, b, **]

[a] State Key Laboratory for Structural Chemistry of Unstable and Stable Species, Beijing National Laboratory for Molecular Sciences (BNLMS), Center for Molecular Sciences, Institute of Chemistry Chinese Academy of Sciences, 100190, Beijing, PR China
[b] University of Chinese Academy of Sciences, Beijing, 100049, PR China
[c] College of Chemical Engineering, North China University of Science and Technology, Hebei, Tangshan, 063210, PR China

ARTICLE INFO

Article history:
Received 12 March 2019
Accepted 17 April 2019
Available online 23 April 2019

Keywords:
G-quadruplex
Ligands
Living cells
Selective binding
Fluorescent probe

ABSTRACT

G-quadruplex has been an emerging target for drug design due to its physiologically important roles in oncology. A number of quadruplex-interactive ligands have been developed by synthetic and medicinal chemists over the past decades. However, the great challenge still remains that the method for detecting the specific targeting of these ligands to the G-quadruplex structures in cells is still lacking. Herein, a detection system for directly identifying the specific targeting of a ligand to DNA G-quadruplexes in cells was constructed by using a small-molecular fluorescent probe (IMT) as a fluorescent indicator. Four typical ligands have been successfully evaluated, demonstrating the promising application of this detection system in the screening and evaluation of quadruplex-specific therapeutic agents.

1. Introduction

G-quadruplex DNA, an attractive high-order structure formed by guanine-rich nucleic acid sequences [1,2], is putatively present in functional genomic regions such as telomeres, the promoters of important proto-oncogenes, and most growth control genes [3–5]. Convincing studies have implicated the biologically important roles of G-quadruplexes in metabolic processes, including transcription regulation of oncogenes, DNA replication and telomere stability [6–8]. This makes G-quadruplex DNA a promising target for drug design. Intensive research on the screening and evaluation of G-quadruplex ligands has been hugely expanded [9–12], and numerous quadruplex-interactive ligands have been developed over the past two decades [13–17]. One of the quadruplex-interactive compounds, quarfloxin (CX-3543), has entered Phase II clinical trials as a first-in-class candidate for multiple types of cancers [18]. However, despite much progress, one of the biggest challenges in this field still exists. That is, the method for detecting the specific targeting of these ligands to the G-quadruplex structures in cells is still lacking.

It is known that most of the quadruplex-interactive ligands are organic compounds with an extended aromatic core structure that interacts with the G-tetrad ends by π–π stacking [14]. To evaluate the specific targeting of a ligand to G-quadruplexes in cells, the method based on competitive replacement of ligands with a fluorescent probe may be feasible. In this method, the fluorescent probe should also have an extended aromatic planar structure so as to be capable of stacking onto the G-tetrad ends by π-π interaction. And for this, the fluorescent probe DAOTA-M2 has been developed to detect the interactions between a small molecular ligand and G-quadruplexes [19]. However, the DAOTA-M2 detection system relies on the fluorescence lifetime imaging microscopy and longer acquisition time is necessary, which limits its wide application [19].

Lately, we designed a fluorescent probe nominated IMT (Scheme 1), which exhibits a unique property in monitoring DNA G-quadruplexes in live cells [20]. The binding site of IMT on the G-quadruplex structures is located on the terminal G-tetrad, which is identical to the site where most of the ligands act on the G-quadruplex structures. When IMT and a ligand coexist in cells, if the ligand does bind to the G-quadruplexes, competitive displacement

* Corresponding author.
** Corresponding author. State Key Laboratory for Structural Chemistry of Unstable and Stable Species, Beijing National Laboratory for Molecular Sciences (BNLMS), Center for Molecular Sciences, Institute of Chemistry Chinese Academy of Sciences, 100190, Beijing, PR China.
E-mail addresses: zhangsuge88@163.com (S. Zhang), hongxsun@iccas.ac.cn (H. Sun), tangyl@iccas.ac.cn (Y. Tang).

https://doi.org/10.1016/j.acax.2019.100017

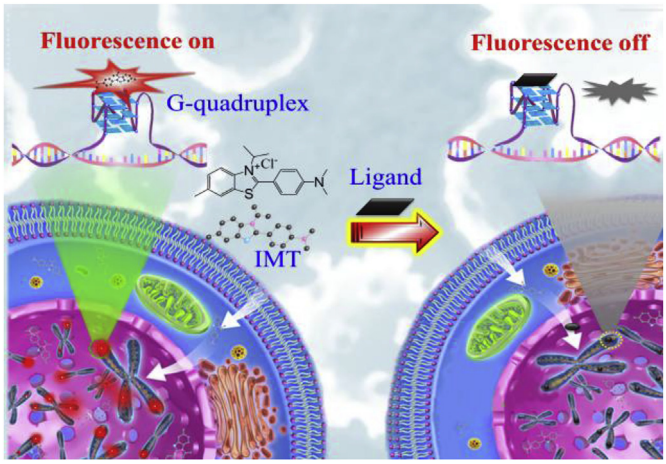

Scheme 1. Schematic representation of IMT as a fluorescent probe to evaluate the specific targeting of ligands to DNA G-quadruplexes in live cells.

of IMT from the quadruplex moiety by ligands is possible (Scheme 1). Thus, changes in IMT fluorescence caused by binding of a ligand to G-quadruplexes can provide direct evidence for ligand-specific targeting of G-quadruplexes in cells. On this basis, the targeting of four typical quadruplex-interactive ligands including pyridostatin (PDS) [21–23], TmPyP4 [24–26], sanguinarine (San) [27,28] and RHPS4 [29,30] has been evaluated by using IMT as a fluorescent indicator.

2. Material and methods

2.1. Sample preparation

All oligonucleotides (Table S1) were purchased from Invitrogen (Beijing, China), purified by PAGE. The stock solutions of the oligonucleotides were prepared by dissolving oligonucleotides directly into 20 mM Tris-HCl buffer (pH 7.0) and annealed in a thermocycler (first heating at 90 °C for 2 min, then cooled down to room temperature slowly). The ligands PDS (NO. SML0678, Sigma), TmPyP4 (NO. 613560, Sigma), San (NO. IS0040, Solarbio) and RHPS4 (NO.B6186, APExBIO, USA) were used as received without further purification. Cell nucleus staining dyes propidium iodide (PI) and SYTO®59 were all obtained from Thermo Fisher Scientific Company. All other ordinary solvents and chemical regents stock solution of IMT (10 mM) was prepared in methanol. Ultrapure water, prepared by Milli-Q Gradient ultrapure water system (Millipore), was used in all experiments.

2.2. UV–vis absorption spectroscopy

Absorption spectra were acquired with UV-1601PC at room temperature using a quartz cuvette with a path length of 10 mm.

2.3. Fluorescence spectroscopy

Fluorescence spectra were acquired using Hitachi F-4600 at room temperature. A 10-mm path length quartz cuvette was used in all experiments. For fluorescence measurements, both excitation and emission slits were 5 nm, and the scan speed was set at 1200 nm min^{-1}.

2.4. Cell culture

Hela (cervical carcinoma) cells were cultured in high glucose DMEM (Dulbecco's Modified Eadle's Medium) containing 10% fetal bovine serum (FBS) and 1% penicillin-streptomycin in 5% CO_2 at 37 °C for 48 h.

2.5. Ligand cytotoxicity

Hela Cells were seeded in 96-well plates (5.0×10^5 cells per well) and exposed to different concentrations of ligands. After 15 min incubation, 20 μL of 5 mg mL^{-1} methylthiazolyl tetrazolium (MTT) solution was introduced to each well, and the cells were further incubated for 4 h. The cells in each well were then treated with dimethyl sulfoxide (DMSO) (200 μL per well), and the optical density (OD) was recorded at 490 nm. All experiments were performed in parallel and in triplicate, and the Cell viability were derived from the curves of the mean OD values of the triplicate tests plotted against the drug concentration.

2.6. Fixed cell imaging

Hela cells grown on Petri dish were fixed for 5 min in cold methanol, rinsed twice with phosphate-buffered saline (PBS), and then incubated with 4 μM IMT and various concentration of ligands (0–16 μM) for 15 min approximately. The nuclei were counterstained with PI. Then cells were visualized under a CLSM (OLYMPUS FV1000-IX81) equipped with an oil immersion 100X objective. CLSM images of IMT and PI were collected under excitation wavelength at 405 nm and 559 nm, respectively.

2.7. Live cell imaging

For living cells, IMT (4 μM) and the ligands with different concentrations of 0–16 μM were added to the culture medium for 15 min before collecting the CLSM images. The red nucleic dye SYTO®59 was used to label the nuclei of living cells. Then cells were visualized under the CLSM. CLSM images of IMT and SYTO®59 were collected under excitation wavelength at 405 nm and 635 nm, respectively.

2.8. Statistical analysis of relative fluorescence intensity

To quantify the fluorescence intensity in the nuclei, the digital images were analyzed using the high content screening (HCS) studio bio-application from the Cellomics ArrayScan Vti (Thermo Fisher Scientific, USA) high-content imaging analysis platform. The data were obtained from approximately 300 cells per sample and the standard error of the mean was calculated from three replicates. Statistical analysis and *P* values were calculated using the Student's-test.

3. Results and discussion

3.1. Ligand screening

Three factors for evaluation of quadruplex-ligands based on the fluorescence competition displacement are critical. That is, the ligands should have the same site as IMT on the G-quadruplex structures; the binding affinity should be high enough for the ligands to replace IMT; and the IMT fluorescence should not be disturbed by the ligand fluorescence. Since the large planar structure has become an important feature that distinguishes G-quadruplex structures from double-stranded DNA, most of the quadruplex-interactive ligands have an extended aromatic core structure, enabling them to be stacked on the G-tetrad plane [14]. Thus most ligands have the same interaction sites on the G-quadruplex structures as IMT. The ligands PDS, TmPyP4, San and RHPS4 with large planar aromatic scaffolds, should also be no exception

[31–36].

To confirm this, we conducted a ligand-induced fluorescence quenching assay. In this assay, differentially Cy5 end-labelled oligonucleotides (oligos) were used to measure 5′-tetrad or/and 3′-tetrad quenching caused by a ligand, thereby validating the ligand binding to either end of a G-quadruplex structure [36]. Three typical G-quadruplex topologies including parallel, antiparallel and hybrid-type were studied as representative (Table S1) [37–40]. For all of these G-quadruplex topologies, the emission intensity of Cy5 only at one end has been quenched by IMT (Fig. S1), indicating that IMT only bound to one tetrad, which is consistent with our previous analysis [20]. However, the emission intensity of Cy5 at both ends have been pronouncedly quenched by the four ligands, revealing that the action site of IMT on the quadruplex structures has also been targeted by these ligands.

According to the fluorometric titrations, the binding constants of the four ligands to various G-quadruplex structures are over $10^6\ M^{-1}$ (Fig. S2), close to the previously reported values [36,41,42]. The binding constant (K_a) of IMT to G-quadruplex structures is about $10^5\ M^{-1}$ [41,42], lower than the K_a values of these four ligands, which means that the ligands can replace IMT from the G-tetrad effectively.

To verify whether the fluorescence emission of the four ligands causes background interference, we subsequently measured the fluorescence characteristics of these ligands in the buffer solution. It is known that the maximum absorbance of IMT is at 405 nm (Fig. S3), so only 405 nm excitation can be selected for cell imaging experiments under CLSM. To mimic the excitation wavelength of CLSM imaging, we performed the fluorescence measurement of all ligands using an excitation wavelength of 405 nm. The fluorescent spectra of all four ligands exhibited negligible fluorescence within the range of 425–525 nm (corresponding to the CLSM fluorescence collection wavebands) (Fig. S4), indicating that these ligands will not interfere with the detection of the IMT fluorescence.

3.2. Ligands replace IMT in solution

Having known that all four ligands meet the above three requirements, we then conducted the competition displacement experiments using ligands to replace IMT from the G-quadruplex structures. For each ligand, we determined the ratio (F/F_0) of the IMT fluorescence signal with the addition of ligands in the presence of different G-quadruplex structures. In any set of samples, the fluorescence of IMT-quadruplex is significantly quenched by the ligands and the fluorescence intensity reduced by more than 70% in the presence of 4-fold ligands (Fig. 1 and S5), confirming the effective displacement of IMT by these ligands. To further understand how long this replacement process takes, time-dependent fluorescence measurement of the IMT-quadruplex adducts was performed once the ligands were titrated in. We found that the fluorescence signal dropped sharply when the ligand was added (Fig. S6) and reached its lowest value within 2 min. The results indicate that the ligand displacement of IMT is a rapid process.

The fluorescence quenching caused by ligand competition allows for the determination of whether a ligand targets G-quadruplexes based on changes in the IMT fluorescence. If the ligand is highly targeted to G-quadruplexes without interference from double-stranded DNA, competition of the ligand with IMT will effectively quench the IMT fluorescence. Conversely, if the ligand also has high affinity for double-stranded DNA, the presence of double-stranded DNA will inevitably reduce fluorescence quenching efficiency. We have observed the effective quenching of IMT fluorescence by the four ligands in the absence of double-stranded DNA. In the presence of 10-fold double-stranded DNA, we found that the efficiency of PDS and RHPS4 quenching IMT fluorescence

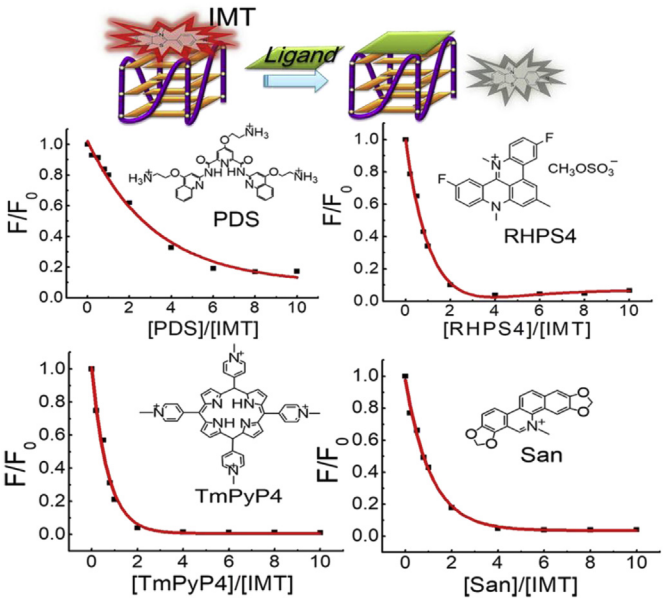

Fig. 1. Fluorescence quenching of IMT (4 μM)–H22 quadruplex (4 μM) by various of ligands in 20 mM Tris-HCl solution (pH 7.0) containing 40 mM KCl. F and F_0 represent the IMT-quadruplex fluorescence intensity at 490 nm with and without ligands, respectively. λex = 405 nm.

was only slightly changed, but the efficiency of TmPyP4 and San quenching IMT fluorescence was significantly reduced (Fig. S7). We further conducted a duplex-titration experiment in the presence of 4-fold ligands and observed a duplex dose-dependent increase in fluorescence of the IMT-quadruplex adducts in the presence of TmPyP4 and San instead of PDS and RHPS4 (Fig. 2). To confirm that the IMT fluorescence enhancement was due to the interaction between IMT and G-quadruplexes after these ligands were competitively bound by the double-stranded DNA, rather than the binding of IMT to the double-stranded DNA, we further determine the fluorescence changes of IMT with an increasing amount of calf thymus (CT)-DNA and herring sperm (HS)-DNA under the condition that IMT is excessive relative to G-quadruplexes. The results showed that the IMT fluorescence only changed slightly after the addition of these double-stranded DNA (Fig. S8), indicating that the fluorescence enhancement of IMT was indeed not due to its interaction with double-stranded DNA. In view of this, we can speculate

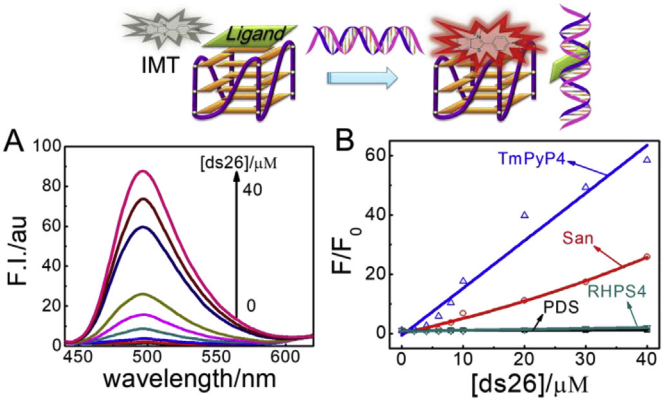

Fig. 2. (A) Fluorescence spectra of IMT (4 μM)–H22 quadruplex (4 μM) with increasing amounts of duplex DNA (ds26) in the presence of TmPyP4 (16 μM). (B) Plots of F/F_0 as a function of [ds26] in the presence of different ligands (16 μM). F and F_0 represent the IMT-quadruplex fluorescence intensity at 490 nm with and without duplex DNA, respectively. All the samples were measured in 20 mM Tris-HCl buffer solution (pH 7.0) containing 40 mM KCl. λex = 405 nm.

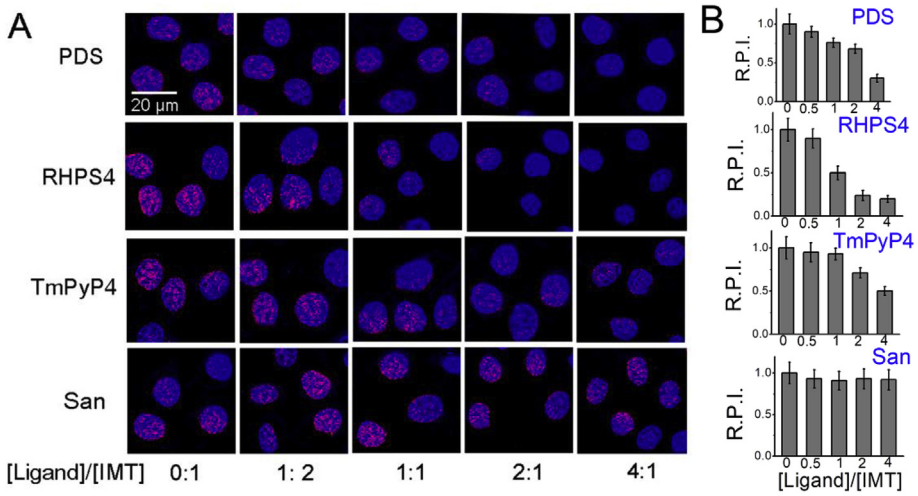

Fig. 3. (A) CLSM images of fixed Hela cells stained by IMT (4 μM) with increasing concentrations of ligands (0–16 μM). For clarity, the images were presented in pseudocolors of red (IMT). The nuclei were counterstained with PI (blue). (B) Relative pixel intensity (R.P.I.) corresponding to each ligand group displayed in the below panel (~300 cells were quantified for each sample). The pixel intensity measured without ligand is defined as 1.0. (For interpretation of the references to color in this figure legend, the reader is referred to the Web version of this article.)

that the specificity of TmPyP4 and San targeting G-quadruplexes may be disturbed by the presence of double-stranded DNA.

3.3. Evaluation of ligands in fixed cells

It is known that the intracellular environment is different from the buffer solution. The ligand targeting to G-quadruplex structures can be more accurately evaluated by directly observing the IMT fluorescence quenching in cells with addition of ligands. Considering that these ligands enter the nucleus may be affected by their membrane permeability, we first performed the evaluation experiments in the fixed Hela cells. In the absence of any ligand, we could observe punctate fluorescence foci from the interaction between IMT and G-quadruplexes in the cell nucleus (Fig. 3A) [20]. With the increase of PDS and RHPS4, the fluorescence foci were obviously decreased, consistent with the fluorescence quenching results in buffer solution, demonstrating the good specificity of the two ligands to the G-quadruplexes in cells (Fig. 3A and B). In the presence of TmPyP4, the fluorescence foci were also reduced, but the degree of reduction was much smaller than that in the solution (Fig. 1), indicating that TmPyP4 may also target other substances such as double-stranded DNA [43–45]. And for San, there was almost no change in the fluorescence foci, which suggests that San may not bind to the G-quadruplex structures in cells. In addition to G-quadruplexes, many proteins and RNAs have also been reported to bind to San with high affinity [46–50], which may be the reason why San cannot target G-quadruplexes in cells.

3.4. Evaluation of ligands in living cells

To further reveal the true targeting of these ligands in biological systems, we then performed live cell imaging in the presence of IMT and ligands. To rule out the toxic damage that these ligands may have on the cells, we performed imaging immediately after 15 min of ligand addition. MTT experiments confirmed that these ligands did not cause toxic damage to the cells during this period (Fig. S9). The results of live-cell imaging of PDS, San and TmPyP4 were consistent with their results in fixed-cell imaging (Fig. 4). For

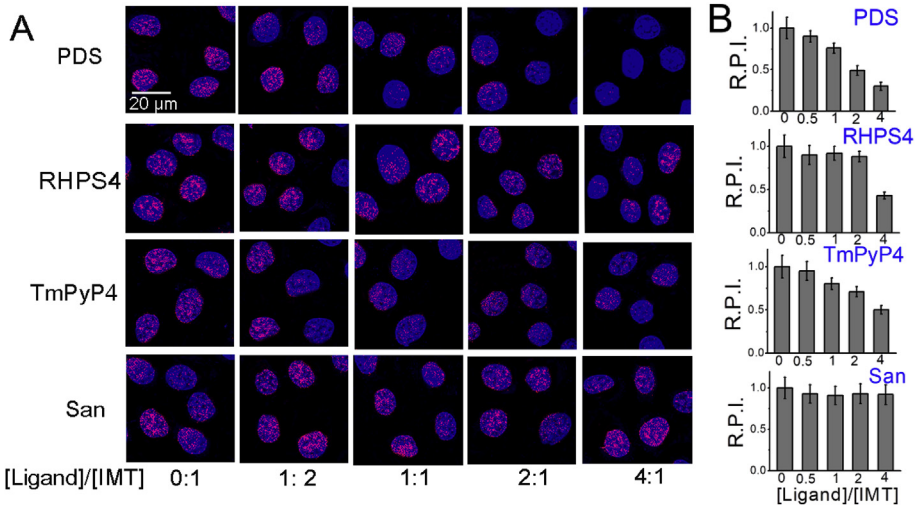

Fig. 4. (A) CLSM images of living Hela cells stained by IMT (4 μM) with increasing concentrations of ligands (0–16 μM). For clarity, the images were presented in pseudocolors of red (IMT). The nuclei were counterstained with SYTO®59 (blue). (B) Relative pixel intensity (R.P.I.) corresponding to each ligand group displayed in the below panel (~300 cells were quantified for each sample). The pixel intensity measured without ligands is defined as 1.0. (For interpretation of the references to color in this figure legend, the reader is referred to the Web version of this article.)

the RHPS4 group, however, the fluorescence quenching in live cells was much weaker than that in fixed cells. The main difference between living cells and fixed cells is that they have different permeability. We examined the localization of RHPS4 in both fixed and living cells, and found that RHPS4 was mainly distributed in the nucleus of fixed cells and the cytoplasm of living cells (Fig. S10). The poor membrane permeability of RHPS4 may be the main reason for the decrease of fluorescence quenching efficiency in the live cells.

4. Conclusion

In conclusion, we have provided an effective detection system to directly identify the specificity of ligands to DNA G-quadruplex structures in cells by using IMT as a fluorescent indicator. This detection system is primarily based on the competitive interaction of ligands with IMT on the G-quadruplex structures. The targeting of four typical ligands including PDS, TmPyP4, San and RHPS4 to G-quadruplexes in cells has been evaluated. So far, the development of quadruplex-interactive ligands has become an important research field because of the important regulating roles of G-quadruplexes in tumor and other diseases. Numerous quadruplex-interactive ligands have been developed, but their specificity for G-quadruplexes in vivo has not been well characterized. This study demonstrates the promising application of this detection system in the screening and evaluation of therapeutic agents that specifically target G-quadruplexes in cells.

Conflict of interest

We declare that we have no competing financial interests and personal relationships with other people or organizations that can inappropriately influence our work.

Acknowledgements

This research was supported by Beijing Natural Science Foundation (7182189and 7172248), the National Natural Science Foundation of China (Grant No. 21675162, 21603071 and 21778058), and the Science and Technology Service Program (STS Program) of the Chinese Academy of Sciences (KFJ-STS-QYZX-038).

Appendix A. Supplementary data

Supplementary data to this article can be found online at https://doi.org/10.1016/j.acax.2019.100017.

References

[1] G.N. Parkinson, M.P.H. Lee, S. Neidle, Crystal structure of parallel quadruplexes from human telomeric DNA, Nature 417 (2002) 876–880.
[2] R. Hänsel-Hertsch, M.D. Antonio, S. Balasubramanian, DNA G-quadruplexes in the human genome: detection, functions and therapeutic potential, Nat. Rev. Mol. Cell Biol. (2017) 279–284.
[3] D. Rhodes, H.J. Lipps, G-quadruplexes and their regulatory roles in biology, Nucleic Acids Res. 43 (2015) 8627–8637.
[4] R. Hänsel-Hertsch, D. Beraldi, S.V. Lensing, G. Marsico, K. Zyner, A. Parry, M. Di Antonio, J. Pike, H. Kimura, M. Narita, D. Tannahill, S. Balasubramanian, G-quadruplex structures mark human regulatory chromatin, Nat. Genet. 48 (2016) 1267–1272.
[5] Y. Zhao, J.Y. Zhang, Z.Y. Zhang, T.J. Tong, Y.H. Hao, Z. Tan, Real-time detection reveals responsive cotranscriptional formation of persistent intramolecular DNA and intermolecular DNA:RNA hybrid G-quadruplexes stabilized by R-Loop, Anal. Chem. 89 (2017) 6036–6042.
[6] J. Bidzinska, G. Cimino-Reale, N. Zaffaroni, M. Folini, G-quadruplex structures in the human genome as novel therapeutic targets, Molecules 18 (2013) 12368–12395.
[7] S. Balasubramanian, L.H. Hurley, S. Neidle, Targeting G-quadruplexes in gene promoters: a novel anticancer strategy? Nat. Rev. Drug Discov. 10 (2011) 261–275.
[8] C. Zhang, H.H. Liu, K.W. Zheng, Y.H. Hao, Z. Tan, DNA G-quadruplex formation in response to remote downstream transcription activity: long-range sensing and signal transducing in DNA double helix, Nucleic Acids Res. 41 (2013) 7144–7152.
[9] D. Musumeci, J. Amato, A. Randazzo, E. Novellino, C. Giancola, D. Montesarchio, B. Pagano, G-quadruplex on oligo affinity support (G4-OAS): an easy affinity chromatography-based assay for the screening of G-quadruplex ligands, Anal. Chem. 86 (2014) 4126–4130.
[10] Q.J. Zhou, L. Li, J.F. Xiang, Y.L. Tang, H. Zhang, S. Yang, Q. Li, Q.F. Yang, G.Z. Xu, Screening potential antitumor agents from natural plant extracts by G-quadruplex recognition and NMR methods, Angew. Chem. Int. Ed. 47 (2008) 5590–5592.
[11] C. Platella, D. Musumeci, A. Arciello, F. Doria, M. Freccero, A. Randazzo, J. Amato, B. Pagano, D. Montesarchio, Controlled Pore Glass-based oligonucleotide affinity support: towards High Throughput Screening methods for the identification of conformation-selective G-quadruplex ligands, Anal. Chim. Acta 1030 (2018) 133–141.
[12] J. Jamroskovic, M. Livendahl, J. Eriksson, E. Chorell, N. Sabouri, Identification of compounds that selectively stabilize specific G-quadruplex structures by using a Thioflavin T-displacement assay as a tool, Chem. Eur J. 22 (2016) 18932–18943.
[13] S. Neidle, Quadruplex nucleic acids as novel therapeutic targets, J. Med. Chem. 59 (2016) 5987–6011.
[14] P. Murat, Y. Singh, E. Defrancq, Methods for investigating G-quadruplex DNA/ligand interactions, Chem. Soc. Rev. 40 (2011) 5293–5307.
[15] Q. Li, J.F. Xiang, Q.F. Yang, H.X. Sun, A.J. Guan, Y.L. Tang, G4LDB: a database for discovering and studying G-quadruplex ligands, Nucleic Acids Res. 41 (2013) D1115–D1123.
[16] D.L. Ma, D.S.H. Chan, C.H. Leung, Molecular docking for virtual screening of natural product databases, Chem. Sci. 2 (2011) 1656–1665.
[17] S.R. Wu, L.L. Wang, N. Zhang, Y. Liu, W. Zheng, A. Chang, F.Y. Wang, S.Q. Li, D.H. Shangguan, A Bis(methylpiperazinylstyryl)phenanthroline as a fluorescent ligand for G-quadruplexes, Chem. Eur J. 22 (2016) 6037–6047.
[18] D. Drygin, A. Siddiqui-Jain, S. O'Brien, M. Schwaebe, A. Lin, J. Bliesath, C.B. Ho, C. Proffitt, K. Trent, J.P. Whitten, J.K. Lim, D. Von Hoff, K. Anderes, W.G. Rice, Anticancer activity of CX-3543: a direct inhibitor of rRNA biogenesis, Cancer Res. 69 (2009) 7653–7661.
[19] A. Shivalingam, M.A. Izquierdo, A. Marois, A.M. Le, K. Vyšniauskas, K. Suhling, M.K. Kuimova, R. Vilar, The interactions between a small molecule and G-quadruplexes are visualized by fluorescence lifetime imaging microscopy, Nat. Commun. 6 (2015) 8178.
[20] S.G. Zhang, H.X. Sun, L.X. Wang, Y. Liu, H.B. Chen, Q. Li, A.J. Guan, M.R. Liu, Y.L. Tang, Real-time monitoring of DNA G-quadruplexes in living cells with a small-molecule fluorescent probe, Nucleic Acids Res. 46 (2018) 7522–7532.
[21] G. Biffi, D. Tannahill, J. McCafferty, S. Balasubramanian, Quantitative visualization of DNA G-quadruplex structures in human cells, Nat. Chem. 5 (2013) 182–186.
[22] K.I.E. McLuckie, M.D. Antonio, H. Zecchini, J. Xian, C. Caldas, B.F. Krippendorff, D. Tannahill, C. Lowe, S. Balasubramanian, G-quadruplex DNA as a molecular target for induced synthetic lethality in cancer cells, J. Am. Chem. Soc. 135 (2013) 9640–9643.
[23] R. Rodriguez, S. Müller, J.A. Yeoman, C. Trentesaux, J.F. Riou, S. Balasubramanian, A novel small molecule that alters shelterin integrity and triggers a DNA-damage response at telomeres, J. Am. Chem. Soc. 130 (2008) 15758–15759.
[24] F.X. Han, R.T. Wheelhousem, L.H. Hurley, Interactions of TMPyP4 and TMPyP2 with quadruplex DNA. Structural basis for the differential effects on telomerase inhibition, J. Am. Chem. Soc. 121 (1999) 3561–3570.
[25] Y. Mikami-Terao, M. Akiyama, Y. Yuza, T. Yanagisawa, O. Yamada, H. Yamada, Antitumor activity of G-quadruplex–interactive agent TMPyP4 in K562 leukemic cells, Cancer Lett. 261 (2008) 226–234.
[26] A. Siddiqui-Jain, C.L. Grand, D.J. Bearss, L.H. Hurley, VEGF-Trap: a VEGF blocker with potent antitumor effects, Proc. Natl. Acad. Sci. U. S. A 99 (2002) 11593–11598.
[27] K. Padmapriya, R. Barthwal, NMR based structural studies decipher stacking of the alkaloid coralyne to terminal guanines at two different sites in parallel G-quadruplex DNA, $[d(TTGGGGT)]_4$ and $[d(TTAGGGT)]_4$, BBA-Gen. Subjects 1861 (2017) 37–48.
[28] Y.X. Xiong, Z.S. Huang, J.H. Tan, Targeting G-quadruplex nucleic acids with heterocyclic alkaloids and their derivatives, Eur. J. Med. Chem. 97 (2015) 538–551.
[29] E. Salvati, C. Leonetti, A. Rizzo, M. Scarsella, M. Mottolese, R. Galati, I. Sperduti, M.F.G. Stevens, M. D'Incalci, M. Blasco, G. Chiorino, S. Bauwens, B. Horard, E. Gilson, A. Stoppacciaro, G. Zupi, A. Biroccio, Telomere damage induced by the G-quadruplex ligand RHPS4 has an antitumor effect, J. Clin. Investig. 117 (2017) 3236–3247.
[30] J.C. Cookson, F. Dai, V. Smith, R. Heald, A.C.A. Laughton, M.F.G. Stevens, A.M. Burger, Pharmacodynamics of the G-quadruplex-stabilizing telomerase inhibitor 3,11-Difluoro-6,8,13-trimethyl-8H-quino[4,3,2-kl]acridinium methosulfate (RHPS4) in vitro: activity in human tumor cells correlates with telomere length and can be enhanced, or antagonized, with cytotoxic agents, Mol. Pharmacol. 68 (2005) 1551–1558.
[31] J. Husby, A.K. Todd, J.A. Platts, S. Neidle, Small-molecule G-quadruplex interactions: systematic exploration of conformational space using multiple molecular dynamics, Biopolymers 99 (2013) 989–1005.
[32] G.N. Parkinson, R. Ghosh, S. Neidle, Structural basis for binding of porphyrin to

human telomeres, Biochemistry 46 (2007) 2390–2397.
[33] I. Bessi, C. Bazzicalupi, C. Richter, H.R.A. Jonker, K. Saxena, C. Sissi, M. Chioccioli, S. Bianco, A.R. Bilia, H. Schwalbe, P. Gratteri, Spectroscopic, molecular modeling, and NMR-spectroscopic investigation of the binding mode of the natural alkaloids berberine and sanguinarine to human telomeric G-quadruplex DNA, ACS Chem. Biol. 7 (2012) 1109–1119.
[34] C.Y. Wei, G.Q. Jia, J. Zhou, G.Y. Han, C. Li, Evidence for the binding mode of porphyrins to G-quadruplex DNA, Phys. Chem. Chem. Phys. 11 (2009) 4025–4032.
[35] E. Gavathiotis, R.A. Heald, M.F.G. Stevens, M.S. Searle, Recognition and stabilization of quadruplex DNA by a potent new telomerase inhibitor: NMR studies of the 2:1 complex of a pentacyclic methylacridinium cation with $d(TTAGGGT)_4$, Angew. Chem. Int. Ed. 40 (2001) 4749–4751.
[36] D.D. Le, M. Di Antonio, L.K.M. Chan, S. Balasubramanian, G-quadruplex ligands exhibit differential G-tetrad selectivity, Chem. Commun. 51 (2015) 8048–8050.
[37] S. Burge, G.N. Parkinson, P. Hazel, A.K. Todd, S. Neidle, Quadruplex DNA: sequence, topology and structure, Nucleic Acids Res. 34 (2006) 5402–5415.
[38] J. Dai, T.S. Dexheimer, D. Chen, M. Carver, A. Ambrus, R.A. Jones, D. Yang, An intramolecular G-quadruplex structure with mixed parallel/antiparallel G-strands formed in the human BCL-2 promoter region in solution, J. Am. Chem. Soc. 128 (2006) 1096–1098.
[39] A.T. Phan, V. Kuryavyi, S. Burge, S. Neidle, D.J. Patel, Structure of an unprecedented G-quadruplex scaffold in the human c-kit promoter, J. Am. Chem. Soc. 129 (2007) 4386–4392.
[40] Y. Wang, D.J. Patel, Solution structure of the human telomeric repeat d $[AG_3(T_2AG_3)_3]$ G-tetraplex, Structure 1 (1993) 263–282.
[41] K. Bhadra, G.S. Kumar, Interaction of berberine, palmatine, coralyne, and sanguinarine to quadruplex DNA: a comparative spectroscopic and calorimetric study, BBA-Gen. Subjects 1810 (2011) 485–496.
[42] K. Mulholland, F. Siddiquei, C. Wu, Binding modes and pathway of RHPS4 to human telomeric G-quadruplex and duplex DNA probed by all-atom molecular dynamics simulations with explicit solvent, Phys. Chem. Chem. Phys. 19 (2017) 18685–18694.
[43] A. Arora, S. Maiti, Effect of loop orientation on quadruplex–TMPyP4 interaction, J. Phys. Chem. B 112 (2008) 8151–8159.
[44] S. Cogoi, L.E. Xodo, Enhanced G4-DNA binding of 5,10,15,20(*N*-propyl-4-pyridyl) porphyrin (TPrPyP4): a comparative study with TMPyP4, Chem. Commun. 46 (2010) 7364–7366.
[45] R.J. Fiel, Porphyrin—nucleic acid interactions: a review, J. Biomol. Struct. Dyn. 6 (1986) 1259–1274.
[46] A.Y. Khan, G.S. Kumar, Natural isoquinoline alkaloids: binding aspects to functional proteins, serum albumins, hemoglobin, and lysozyme, Biophys. Rev. 7 (2015) 407–420.
[47] M. Hossain, A.Y. Khan, G.S. Kumar, Interaction of the anticancer plant alkaloid sanguinarine with bovine serum albumin, PLoS One 6 (2011) e18333.
[48] G.S. Kumar, S. Hazra, Sanguinarine, a promising anticancer therapeutic: photochemical and nucleic acid binding properties, RSC Adv. 4 (2014) 56518–56531.
[49] M. Lopus, D. Panda, The benzophenanthridine alkaloid sanguinarine perturbs microtubule assembly dynamics through tubulin binding, FEBS J. 273 (2006) 2139–2150.
[50] L.P. Bai, Z.Z. Zhao, Z.W. Cai, Z.H. Jiang, DNA-binding affinities and sequence selectivity of quaternary benzophenanthridine alkaloids sanguinarine, chelerythrine, and nitidine, Bioorg. Med. Chem. 14 (2006) 5439–5445.